J. Iron Steel Res. Int. (2023) 30:487–503
https://doi.org/10.1007/s42243-022-00879-0

ORIGINAL PAPER

Effect of die structure parameters on deformation behavior of bent tube in free bending process

Wei Wang[1] · Cheng Cheng[1,2] · Li Wan[3] · Jie Tao[1] · Xun-zhong Guo[1] · Chun-mei Liu[1]

Received: 18 March 2022 / Revised: 26 June 2022 / Accepted: 22 August 2022 / Published online: 18 December 2022

Abstract

The bending section of tube between the bending die and the guider is in a less constrained state during the free bending process. The free bending dies have the important impact on the plastic deformation behavior and the forming quality of tube. To study the evolution law of the deformation behavior of tube with the die structure parameters and optimize the free bending die parameters, the free bending experiments and the corresponding numerical simulations were carried out. The design principle of free bending die was illustrated. The free bending experiment was conducted to verify the reliability of the numerical simulation method. Based on the numerical simulation results, the influence of the distance between the center point of bending die and the front end of guider on the forming quality of bent tube is more obvious than that of the fillet of guider. However, the fillet of bending die hardly affects the stress and strain distribution and the evolution of the wall thickness. Finally, the free bending experiments with the newly determined free bending dies were conducted. The ultimate bending radius of bent tube is reduced and the forming quality is improved.

Keywords Free bending · Die structure parameter · Forming quality · Numerical simulation · Tube

1 Introduction

Due to the advantages of lightweight, high strength and flexibility, metal tubes with complex spatial shapes are widely used in aerospace, automotive, rail traffic and other industrial fields [1–3]. Considering the limitation of the space layout, the original metal tube needs to be bent into the complex shape with different bending radii and angles. At present, bending forming technologies, such as the rotary draw bending [4], the tension bending [5] and the roll bending [6], can be used to manufacture the bent tubes. However, the above traditional bending forming technologies are difficult to realize the integral forming of bent tubes with variable curvature axes. The free bending technology has been studied extensively in recent years [7]. By controlling the spatial position and posture of the free bending die and exerting the axial feeding motion on the original tube, the bent tubes with complex axial shapes can be formed. This technology can realize the continuous change of the bending radius and angle in the bent tube without replacing the bending die, which greatly improves the forming efficiency of the complex bent tube and reduces the cost of die manufacturing.

Since the shape of formed bent tube is directly determined by the spatial position of bending die, many scholars focused on the relationship between the axial shape of bent tube and the spatial position of bending die. For example, three-dimensional free bending technology was first proposed by Murata et al. [8, 9]. Its basic principle was verified, and the relationship curve between the bending die deflection U and the bending radius R of bent tube was established by the free bending forming experiment [10, 11]. Gantner et al. [12] developed the free bending

✉ Cheng Cheng
c_cheng@nuaa.edu.cn

✉ Jie Tao
taojie@nuaa.edu.cn

[1] College of Material Science and Technology, Nanjing University of Aeronautics and Astronautics, Nanjing 211100, Jiangsu, China

[2] State Key Laboratory of Digital Manufacturing Equipment and Technology, Huazhong University of Science and Technology, Wuhan 430074, Hubei, China

[3] Capital Aerospace Machinery Corporation, Beijing 100076, China

forming equipment. By comparing the numerical simulation and experimental results, it was proven that the free bending forming process can be characterized by the finite element method (FEM). Subsequently, Gantner et al. [13] studied the relationship between the bending radius of tube and the bending die deflection and proposed an analytical equation for the bent tube with complex axis shape. Kawasumi et al. [14] developed the free bending forming equipment based on the parallel mechanism. The spatial posture of bending die could be actively adjusted by changing the length of the robotic arm. The geometric relationship between the shape of formed bent tube and the parallel mechanism was also explored. Chatti et al. [15] proposed a new torque superposed spatial (TSS) bending forming technology for profiles with different cross section shapes. To obtain the complex workpieces with different bending and torsional features, the torque was superposed on the bending moment and their geometrical mapping to bending-torsional features was studied.

Furthermore, many researchers have studied the influence of forming process parameters and material properties on the forming quality of bent tubes during the free bending forming process. For example, Xiong [16] investigated the effects of material parameters on the *U–R* relationship by carrying out the sensitivity analysis. The bending radius of bent tube decreases and the degree of plastic deformation increases with the increase in the elastic modulus, strain-hardening exponent and decreasing the yield stress of material. Li et al. [17, 18] studied the influence of process parameters (friction, clearance and mobile die section shape) on the springback behavior of bent tube during the process of free bending. The analytical model of tube bending springback was optimized by introducing the additional neutral layer offset. To optimize the forming process parameters for bent tubes with the complex spatial axes, Zhang et al. [19] analyzed the characteristics of stable elements and unstable elements of bent tube and established a mathematical collection for describing the geometrical characteristics of unstable elements. Guo et al. [20] used the method of inserting a mandrel inside tube to eliminate the cross-sectional distortion and the axial instability of bent tube during the process of free bending forming. The optimized mandrel parameters were determined to promote the bending quality of the thin-walled tube. Chen et al. [21] explored the impact of the wall thickness of tube on the bending behavior of the AA6061 tube in the free bending process. It was found that the maximum equivalent stress decreased when the relative thickness was set as 0.067.

Considering that the bending section of the bent tube between the bending die and the guider is in a less constrained state during the process of free bending, the plastic deformation behavior of bent tube is directly affected by the die structure parameters. However, there are few studies on the influence of free bending die structure on the forming quality of bent tubes in the process of free bending. Chen et al. [22] studied the influence of the bending die structure on the forming force and the forming quality in the free bending process. It was found that the uniformity of the wall thickness distribution of bent tube along the circumferential direction can be improved by using roller and ball in the bending die. Meng [23] analyzed the impact of the swing die structure and parameters on the bending quality. The structural design and optimization of the swing die for the joint swing free bending process were carried out by the finite element simulation and orthogonal analysis. To realize the free bending of bent tube with smaller bending radius, Guo et al. [24] designed a new set of spherical connection between the bending die and the guider and analyzed the formation mechanism of the curved arc of bent tube. In addition, many scholars have directly explained the specific bending die parameters in their researches on free bending process. For example, Wu and Zhang [25] studied the springback compensation strategy in flexible bending process and the distance between the mobile die and the rotation center was set as 55 mm for the 6061 aluminum alloy tube with the diameter of 10 mm. Maier et al. [26] analyzed the influence of process parameters on residual stresses for six-axis free-form bending with movable die. The distance along *Z*-direction between the center of the moving bending die and the end of the guider is 56 mm for the welded steel tubes with the outer diameter of 42.4 mm. Hashemi and Niknam [27] investigated the effect of key parameters on the bending radius in the free bending process of rectangular copper profiles. The fixed die fillet was considered to be 4 mm, and the distance between the center of the fixed die and the moving die was about 32 mm.

However, the previous studies on the free bending only analyzed the deformation behavior of bent tube under the specific die structure parameters and did not consider the influence of changes in die structure parameters on the forming quality and ultimate bending radius. This paper mainly focused on the impact of die structure parameters on the deformation behavior of bent tube in the free bending process. The forming principle of free bending and the formation mechanism of curved arc were analyzed. Based on the free bending forming experiment and numerical simulation, the evolution laws of the bending radius, the stress–strain state and the wall thickness distribution with the die structure parameters were discussed. Finally, the determination principle of die structure parameters has been put forward.

2 Forming principle of three-dimensional free bending

2.1 Brief description of free bending process

The principle diagram of the free bending forming of tube is shown in Fig. 1. The free bending forming system consists of five parts: spherical bearing, bending die, guider, feeding device and pressing tool. During the process of free bending, the original tube moves first along the Z-axis under the action of the feeding device. Then, the straight tube is bent into the corresponding bending arc when it passes through the guider and the bending die. The length between the center point of bending die and the front end of guider in X–Y projection plane is called as the deflection U, which could be changed by adjusting the spatial position of bending die. According to the pre-determined motion trajectory of bending die, the complicated shaped bent tube with different bending angles and radii can be deformed. The distance A between the center point of bending die and the front end of guider along Z-axis is fixed, which is determined by the mechanical structure of free bending die, such as the bending die and the guider.

As shown in Fig. 1, $\boldsymbol{P}_{\mathbf{U}}$ is the bending forming force of the movable bending die on the tube during the free bending process, which is perpendicular to the center line of the bent tube. $\boldsymbol{P}_{\mathbf{L}}$ is the propulsive force exerted by the feeding device to tube. Both $\boldsymbol{P}_{\mathbf{U}}$ and $\boldsymbol{P}_{\mathbf{L}}$ are closely related to U and A. Under the combined action of the above-mentioned forces, the tube is bent and deformed, and the moment $\boldsymbol{M}$ can be expressed as:

$$\boldsymbol{M} = \boldsymbol{P}_{\mathbf{L}} \times U + \boldsymbol{P}_{\mathbf{U}} \times A \tag{1}$$

The part of bent tube located inside the bending direction is subjected to the compressive stress along three principal stress directions ($\sigma_\rho, \sigma_\varphi, \sigma_\theta$), which easily causes wrinkling, instability and thickening of the wall thickness on the intrados of bent tube. The part of bent tube located outside the bending direction is under the tangential tensile stress state, and these defects such as the excessive thinning of wall thickness and the cross-sectional distortion easily occur. Furthermore, considering the additional propulsive force exerted by the feeding device, the tangential compressive stress on the inner side of bent tube increases, and the tangential tensile stress on the outer side of bent tube decreases. Therefore, the intrados of bent tube is prone to wrinkling, and the thinning of wall thickness on the extrados of bent tube is alleviated during the process of free bending.

2.2 Forming mechanism of bent tube axis

During the free bending forming process, the formation of bending arc of bent tube is accompanied by the movement of bending die. The single bending arc can be divided into five sections, which correspond to different motion modes of bending die, as shown in Fig. 2. Section 1 is the straight tube. The bending die remains stationary at the origin and the tube does not undergo the plastic deformation. Section 2 is the first transition element. The bending die moves from the initial position to the maximal deflection in the X–Y projection plane. Section 3 is the stable circular arc segment. The bending die remains stationary at the maximal deflection. The tube is fed along the Z-axis, and the stable arc segment is continuously formed. The corresponding bending radius of the stable arc segment is unchanged. Section 4 is the second transition element. The bending die returns to the origin from the maximal deflection. Section 5 is the following line segment.

The formation process of first transition element is shown in Fig. 3a. The bending die is assumed to be perpendicular to the bending axis of bent tube. The arc length S_2 of the first transition element can be calculated as:

$$\begin{cases} \theta_1 = \arcsin A/R \\ S_2 = \dfrac{\pi R \theta_1}{180^\circ} \end{cases} \tag{2}$$

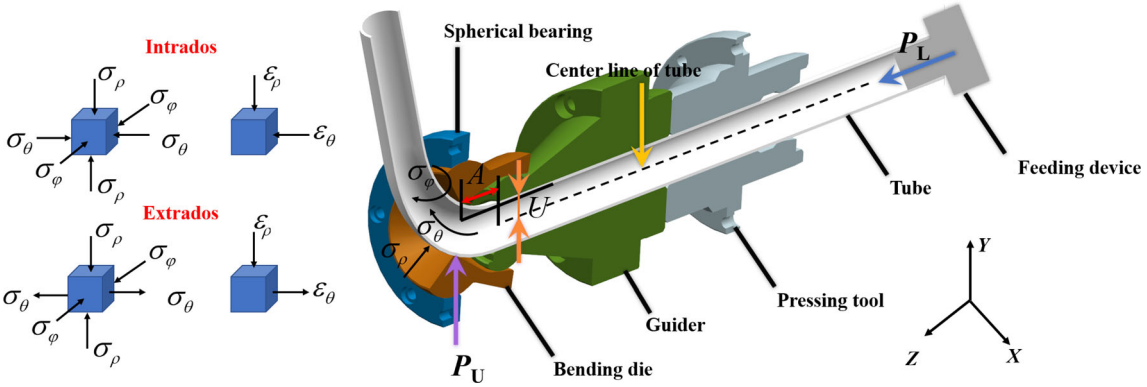

Fig. 1 Schematic illustration of free bending and stress state

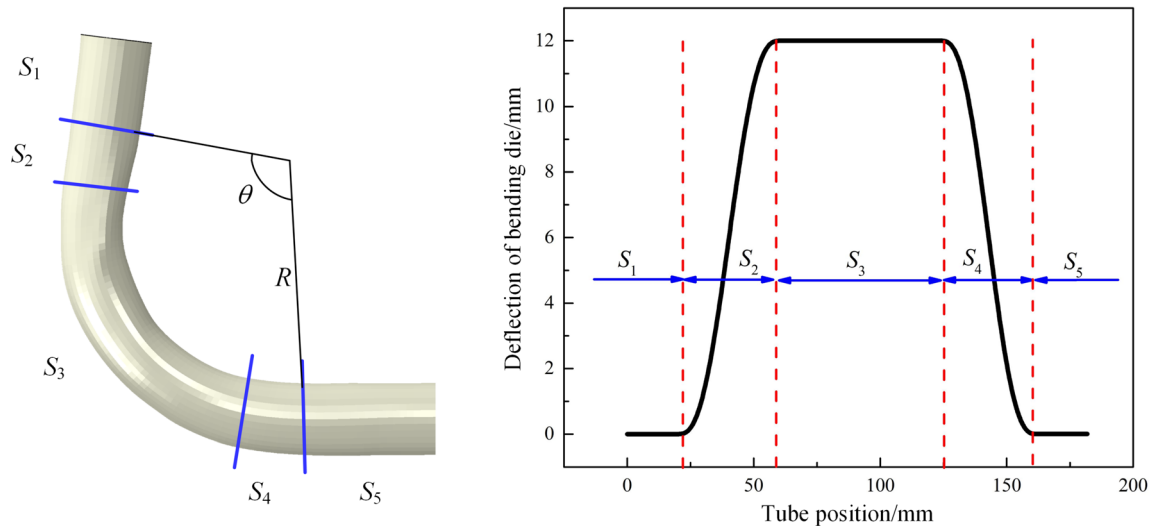

Fig. 2 Description of different sections in single bending arc and corresponding motion process of bending die

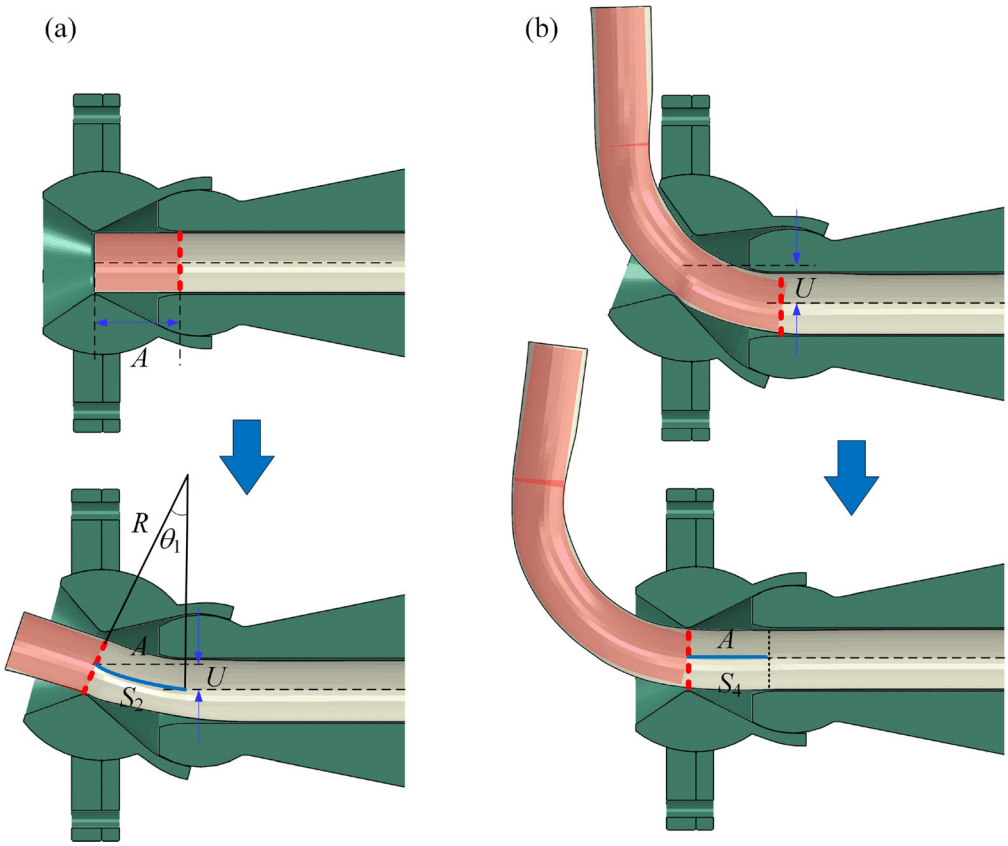

Fig. 3 Schematic diagram of transition element formation. **a** First transition element; **b** second transition element

It could be concluded that the length of first transition element increases with the increase in A. The formation process of second transition element is shown in Fig. 3b. The length S_4 of the second transition element is defined as:

$$S_4 = A \tag{3}$$

As shown in Fig. 2, the length S of the entire arc is written as:

$$S = \frac{\pi R\theta}{180^\circ} \tag{4}$$

According to the study of Gantner et al. [13], the first and second transition elements are contained in the entire

arc segment. If the length of transition element increases, its proportion in the entire arc segment is larger. Since the curvature of the transition element changes continuously, it has a very significant effect on the shape of bent tube. Referring to Fig. 3a, it could be found that both U and A have the impact on the bending radius of the tube, and the theoretical relationship is expressed as:

$$A = \sqrt{2RU - U^2} \tag{5}$$

It can be preliminarily concluded that the bending radius increases and the bending deformation degree of tube decreases with the increase in A under the condition of the same U. In summary, the bent tubes with complex axis shapes are composed of the bending arcs with different bending radii and angles.

3 Free bending experiment and simulation

3.1 Design of die structure parameters

The die structure diagram of free bending forming is shown in Fig. 4. The tube is bent and deformed under the combined action of the free bending dies. Considering that the bending die and the guider are in direct contact with the tube, the structure parameters of the bending die and the guider would affect the bending deformation behavior of bent tube in the free bending process. The assembly relationship between the bending die and the guider is shown in Fig. 4. As we can find, the following spatial position relationship between the bending die and the guider needs to be satisfied. The tail of the bending die **a1** and **a2** cannot be disengaged from the front end of the guider **b1** and **b2** during the free bending process. The collision between the bent tube and the front end of the bending die **c1** and **c2** needs to be avoided. In addition, the front end of the bending die cannot go over the back side of the spherical bearing. To avoid the bending stress concentration of tube caused by the free bending dies, the parts of the forming dies that are in direct contact with the tube are usually designed with the filleted corner, as shown in Fig. 4.

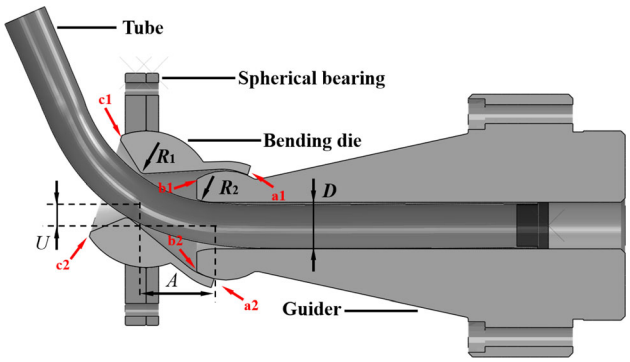

Fig. 4 Die structure diagram of free bending

On the premise of meeting the above design requirements, the radius of filleted corner $\boldsymbol{R_1}$ of bending die, the radius of filleted corner $\boldsymbol{R_2}$ of guider and the distance between the center point of bending die and the front end of guider are the key die structure parameters that affect the forming quality of bent tube. The $\boldsymbol{R_1}$ and $\boldsymbol{R_2}$ are in direct contact with the bent tube. If the filleted corner radius is too small, the strong stress concentration on the intrados of bent tube would introduce a variety of forming defects. When the bending die deflection is the same, the bending radius decreases with decreasing A, and the ultimate bending radius of the bent tube may be reduced. However, if A is too small, the axial instability of the bent tube may occur. Therefore, to ensure the forming quality of bent tube and improve the forming limit of free bending, it is essential to optimize the die structure parameters of free bending forming, including radius of $\boldsymbol{R_1}$, radius of $\boldsymbol{R_2}$ and A. It should be emphasized again that U can be dynamically adjusted by changing the spatial position of the bending die. This paper focused on the influence of die structure parameters, as shown in Table 1, on the deformation behavior of bent tubes in the free bending process.

3.2 Free bending experiment

The three-dimensional free bending experiments were conducted on the three-axial free bending forming equipment developed by Nanjing University of Aeronautics and Astronautics, as shown in Fig. 5. The forming equipment mainly includes the bending die, the spherical bearing, the guider and the pressing tool. The stainless steel SS304 tubes with the diameter of 22 mm and the thickness of 0.90 mm were used for the free bending experiment. The uniaxial tensile tests were carried out on the universal testing machine. The geometry and dimensions of specimens are shown in Fig. 6a. To reduce the accidental error in the experimental process, the tensile tests were repeated three times with reference to the Chinese standard GB/T228-2002. The average flow stress–strain curve of the stainless steel SS304 tube is shown in Fig. 6b. The Hollomon equation shown in Eq. (6) was employed to fit the

Table 1 Design of die structure parameters (mm)

Die structure	Parameter setting
$\boldsymbol{R_1}$	1.5, 3.0, 4.5
$\boldsymbol{R_2}$	22, 42, 62
A	30, 34, 38

Fig. 5 Three-axial free bending forming equipment

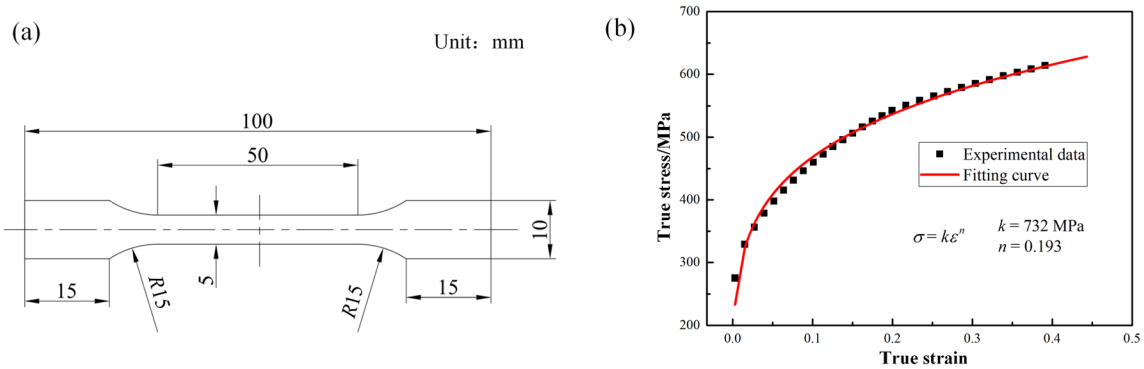

Fig. 6 Uniaxial tensile specimen (**a**) and flow stress–strain curve (**b**) of stainless steel SS304 tube

stress–strain curve. It was found that the fitting theoretical curve is very close to the experimental data, and the model parameters are also given in Fig. 6b.

$$\sigma = k\varepsilon^n \tag{6}$$

where σ is the true stress; ε is the true strain; k is the strength coefficient; and n is the strain hardening exponent.

The original stainless steel SS304 tube was placed in the pressing tool and passed through the guider and the bending die in turn under the action of the feeding device. Subsequently, the straight tube was bent into the pre-designed shape with different bending radii and angles when the position of bending die was continuously adjusted in the X–Y plane. Furthermore, the lubricating oil was used between the bent tube and the free bending dies. The corresponding parameter settings of free bending experiment are summarized in Table 2. $\boldsymbol{R_1}$, $\boldsymbol{R_2}$ and A were set as 3.0, 42 and 38 mm, respectively. The experimental free bending dies are shown in Fig. 7.

3.3 Finite element simulation

To analyze the plastic deformation behavior of the bent tube more conveniently, the finite element simulation of

Table 2 Parameter setting for free bending experiment and simulation

Parameter	Experiment	Simulation
Axial propulsion velocity/(mm s^{-1})	10	10
Tube diameter/mm	22	22
Wall thickness/mm	0.9	0.9
Clearance between tube and die/mm	0.1	0.1
Friction coefficient	Lubricating oil	0.02
U/mm	12	12

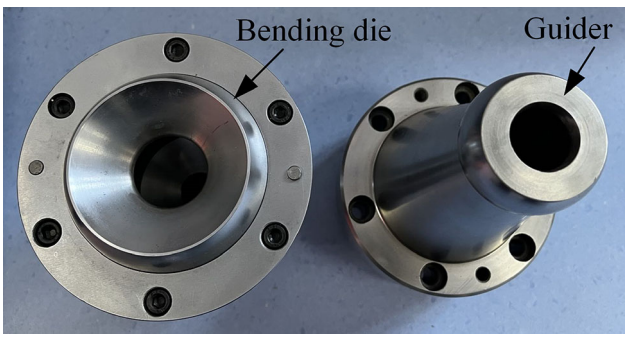

Fig. 7 Experimental free bending dies

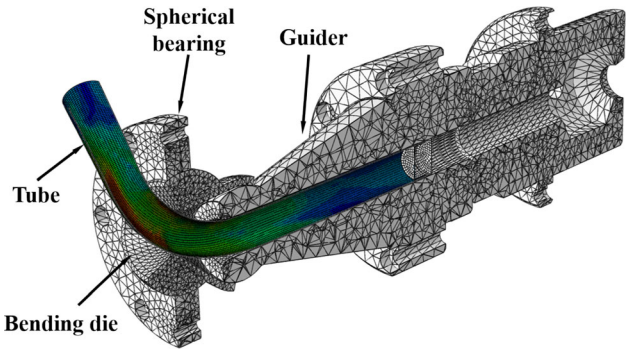

Fig. 8 Finite element model of free bending

the free bending forming process was conducted. As shown in Fig. 8, the finite element model of free bending with different die structure parameters was built in the explicit platform, which includes the bending die, the tube, the spherical bearing and the guider. The tube was defined as the deformable sheet with four-node shell elements (S4R). Since the free bending dies do not undergo the plastic deformation, they can be set as the discrete rigid bodies with the R3D4 elements. The structure of free bending dies can be easily modified in the finite element model. Considering that the lubricating oil was used between different modules, the friction coefficient between the die and the tube was set to be 0.02 in the finite element simulation [28]. Other simulation process parameters are listed in Table 2. The die structure parameters were set according to the free bending experiment in Sect. 3.2. In addition, the stress–strain relationship of stainless steel SS304 tube in Fig. 6 was assigned to the modeled tube.

The free bending experiments were performed three times, and the median of experimental result was adopted. The bent tubes from the free bending experiment and numerical simulation are compared in Fig. 9. It was found that the shape of the simulated bent tube is approximate to the experimental result, and the bending radius of the simulated bent tube is slightly lower than that of the experimental bent tube. To further verify the dependability of the numerical simulation method, the wall thickness distribution and the cross-sectional distortion are shown in Figs. 10 and 11. The experimental and simulated cross-sectional distortion rates are both less than 8.0%. The experimental cross-sectional distortion rate first increases and then decreases with increasing the bending angle of bent tube, which can be accurately characterized by the numerical simulation method. The maximum distortion rate from the free bending experiment is slightly lower than that from the simulation result. The average wall thicknesses of the inner and outer sides of the experimental bent tube are 0.96 and 0.89 mm, respectively. The increase in wall thickness in the intrados of bent tube is significantly greater than the decrease in wall thickness in the extrados of bent tube. This could be because the additional propulsion from the feeding device suppresses the thinning of the bent tube wall thickness. The evolution law of wall thickness from the simulated bent tube with bending angle is similar to that from the experimental bent tube. The difference in thickness between the inner sidewall and the outer sidewall of the simulated bent tube is larger than that from the experimental bent tube. From the comparison results of the simulated and experimental bent tubes, it was inferred that the numerical simulation of free bending may be employed to describe the forming process of free bending of tube.

In the free bending process, the tube is in direct contact with the free bending dies. The bending deformation behavior mainly occurs in the part of bent tube between the bending die and the guider. To better understand the influence of die structure parameters on the deformation behavior of bent tube, the evolution of tangential strain in

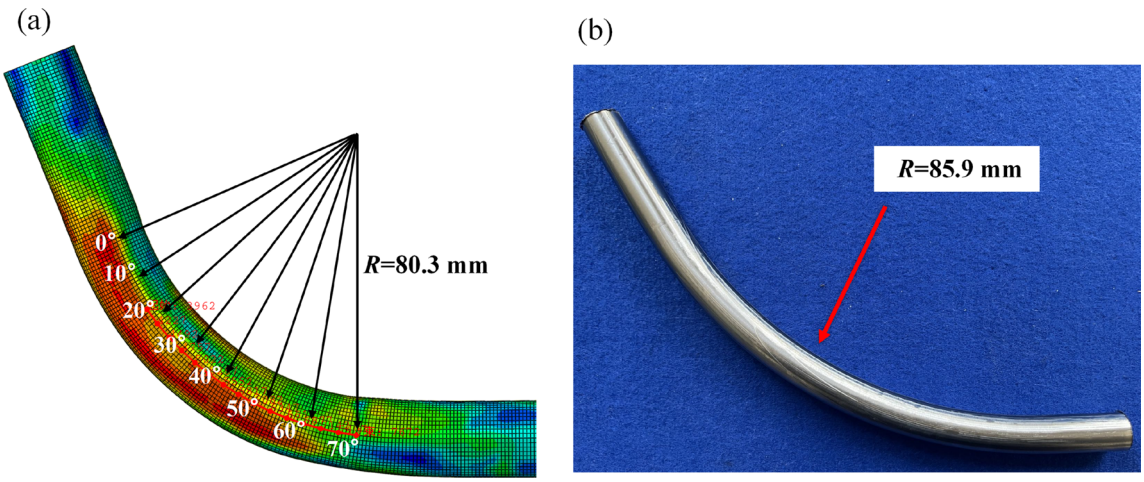

Fig. 9 Comparison of simulated (**a**) and experimental (**b**) bent tubes for free bending

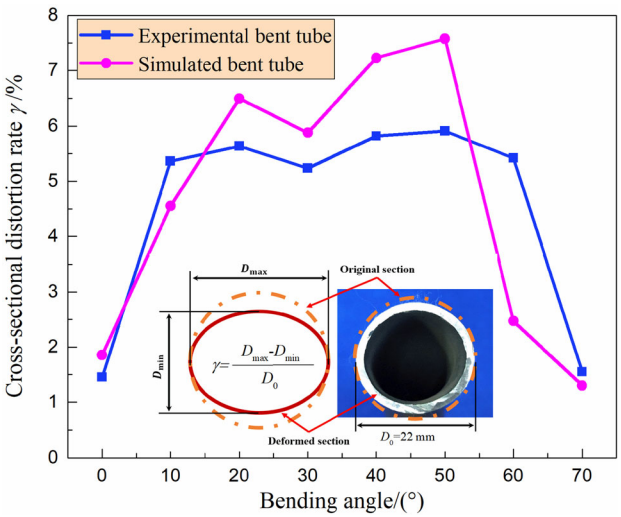

Fig. 10 Comparison of cross-sectional distortion rates of experimental and simulated bent tubes

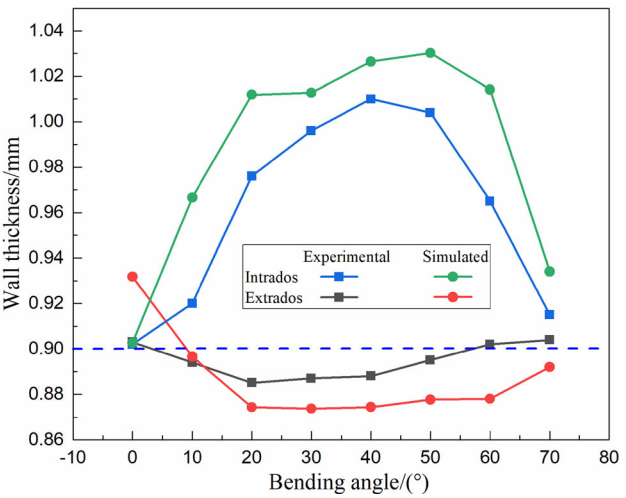

Fig. 11 Comparison of wall thickness distribution of experimental and simulated bent tubes

the intrados and extrados of bent tube with the tube bending line was extracted from Fig. 9. As shown in Fig. 12, the tangential compressive strain on the inside of bent tube increases with the degree of bending deformation. The tangential compressive strain of tube near the filleted corner of guider increases sharply. Subsequently, the tangential compressive strain of tube between the bending die and the guider fluctuates around the maximum value. Similarly, the strain in the outside of bent tube rapidly changes from the initial compressive strain to the tensile strain near the filleted corner of guider. Then, the tangential tensile strain of tube between the bending die and the guider changes slowly. By analyzing the evolution law of tangential strain of tube during the free bending process, it could be concluded that the bending deformation

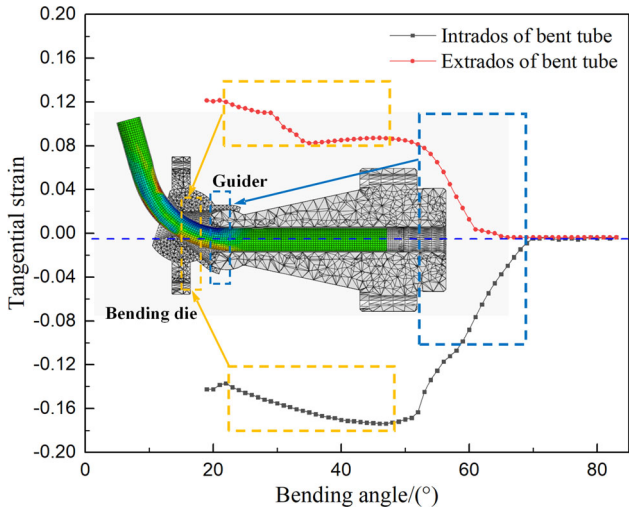

Fig. 12 Evolution of tangential strain in intrados and extrados of bent tube with tube bending line

behavior of tube mainly occurs near the guider. Therefore, it is necessary to investigate the influence of die structure parameters on the deformation behavior of bent tube in the free bending process.

4 Results and discussion

4.1 Influence of *A* on deformation behavior

To study the influence of *A* on the deformation behavior of bent tube, the finite element method was employed to simulate the free bending forming process. The *A* was defined as 30, 34 and 38 mm, respectively, which can be easily adjusted in the finite element model shown in Fig. 8. The simulated stress distribution is shown in Fig. 13. It was found that the maximum equivalent stress is located on the inner side of the bent tube, and it increases gradually as the *A* decreases. The region with higher stress distribution also increases. The above phenomenon may be explained by the bending deformation behavior of bent tube during the free bending process. The degree of plastic deformation of bent tube increases as the *A* decreases. Furthermore, the bending radius increases as the *A* increases under the same *U* of 12 mm, which is consistent with the inference of Eq. (5) that the theoretical bending radius of bent tube decreases with the decrease in *A*. Smaller bending radius results in more severe local plastic deformation. The central angle of bent tube decreases with the increase in *A*. According to Eqs. (2)–(4), the lengths of first transition section and section transition section increase with the increase in *A*, and their proportions in the entire arc segment are also improved. Since the bending radius of transition section is significantly larger than that of the stable arc section, the

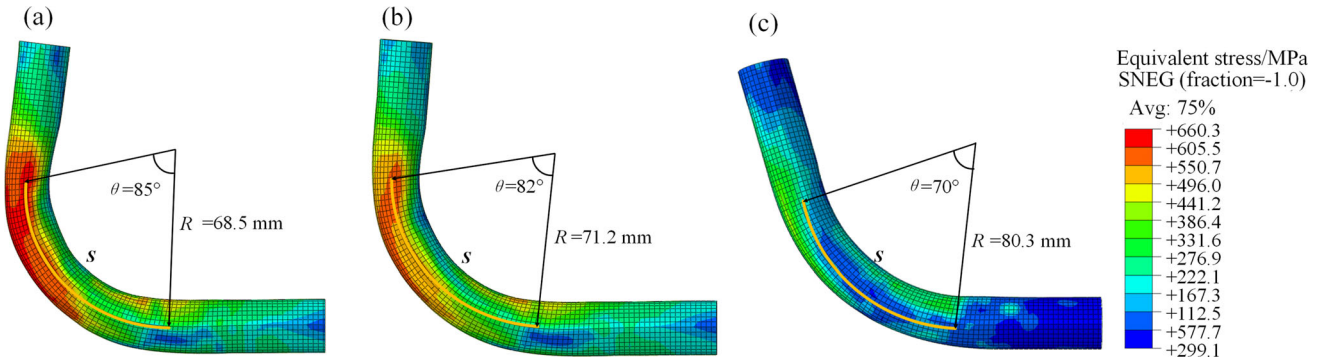

Fig. 13 Equivalent stress distribution cloud maps of bent tubes with different A. **a** A = 30 mm; **b** A = 34 mm; **c** A = 38 mm

average central angle of entire bending arc decreases when the length of entire arc segment is constant. The equivalent strain distributions of the simulated bent tubes with different A are shown in Fig. 14. Similar to the stress distribution result, the maximum equivalent strain decreases with an increase in the distance A.

The wall thickness distributions of bent tubes with different A are shown in Fig. 15. With the decrease in A, the degree of thickening of the wall thickness in the intrados of the bent tube gradually increases. This is because the reduction in the deformation area of bent tube leads to an increase in the force exerted by the feeding device on the tube. The axial propulsion and tangential stress are given in Fig. 16. The tangential compressive stress inside bent tube is larger, which ultimately results in the thickening of the wall thickness in the intrados of bent tube. The axial propulsion increases with the decrease in A, and the degree of thinning of wall thickness in the extrados of bent tube gradually decreases. According to Fig. 17, it could be calculated that the maximum thickening rate of the wall thickness reaches 21.1% when the A is equal to 30 mm, and the wall thickening phenomenon is very significant. The thinning of wall thickness in the extrados of bent tube can even be eliminated when the A is less than 34 mm. Finally, the uniformity of thickness distribution on the inner sidewall and outer sidewall of bent tubes might be enhanced with the smaller A during the free bending process. On the premise that there are no these forming defects, like wrinkling and instability, the improvement in the free bending limit and the reduction in the wall thickness thinning rate can be achieved by reducing A.

To explore the effect of A on the forming limit of tube during the free bending process, the numerical simulation of free bending forming with A of 26 mm was carried out. The simulated bent tube is shown in Fig. 18. It was found that the tube could not be bent without defects. This may be due to the fact that the bending deformation area of bent tube between the bending die and the guider is shortened as A further decreases, and the tube is not easy to pass smoothly the bending die, resulting in the instability of tube between the bending die and the guider. It might be summarized that the forming limit of free bending can be improved and the ultimate bending radius of the bent tube is reduced by appropriately reducing A.

4.2 Influence of R1 on deformation behavior

The simulated equivalent stress of bent tube with different $\boldsymbol{R_1}$ radii is shown in Fig. 19. With the increase in $\boldsymbol{R_1}$, both the compressive stress on the inner sidewall of bent tube and the tensile stress on the outer sidewall of bent tube are slightly reduced. This is because the force exerted by the

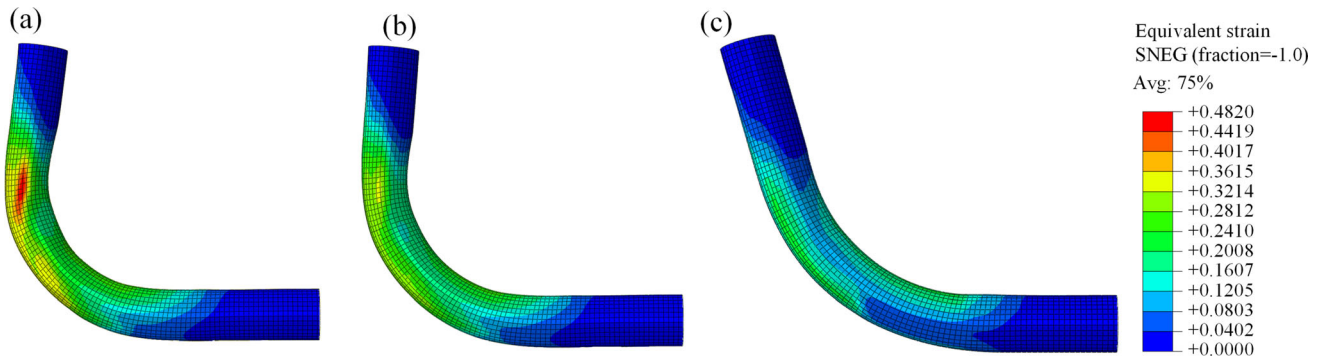

Fig. 14 Equivalent strain distribution cloud maps of bent tubes with different A. **a** A = 30 mm; **b** A = 34 mm; **c** A = 38 mm

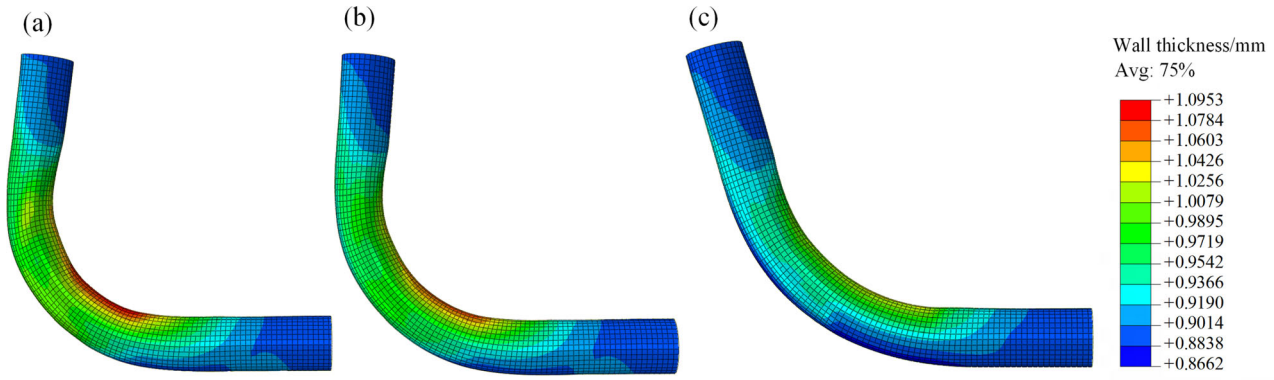

Fig. 15 Wall thickness distribution cloud maps of bent tubes with different A. **a** A = 30 mm; **b** A = 34 mm; **c** A = 38 mm

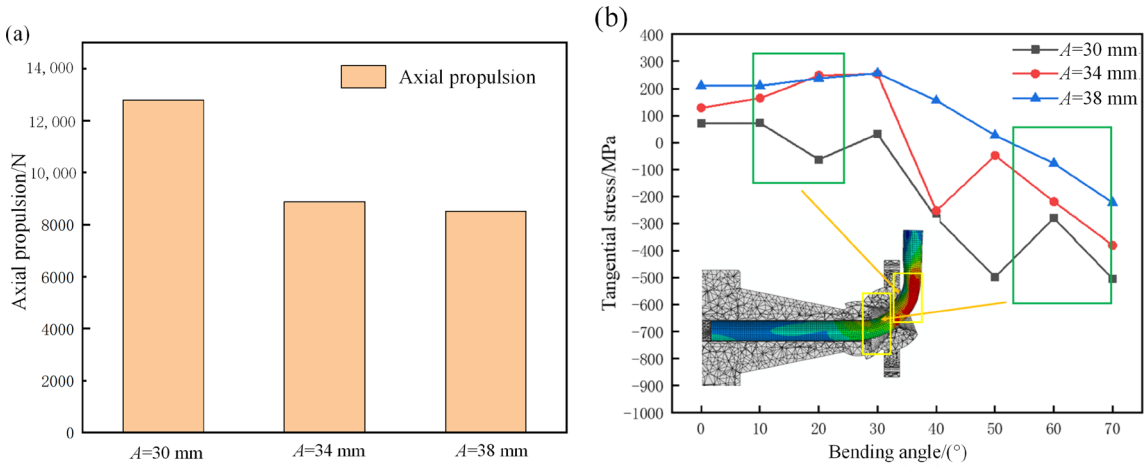

Fig. 16 Axial propulsion (**a**) and tangential stress (**b**) of bent tubes with different A

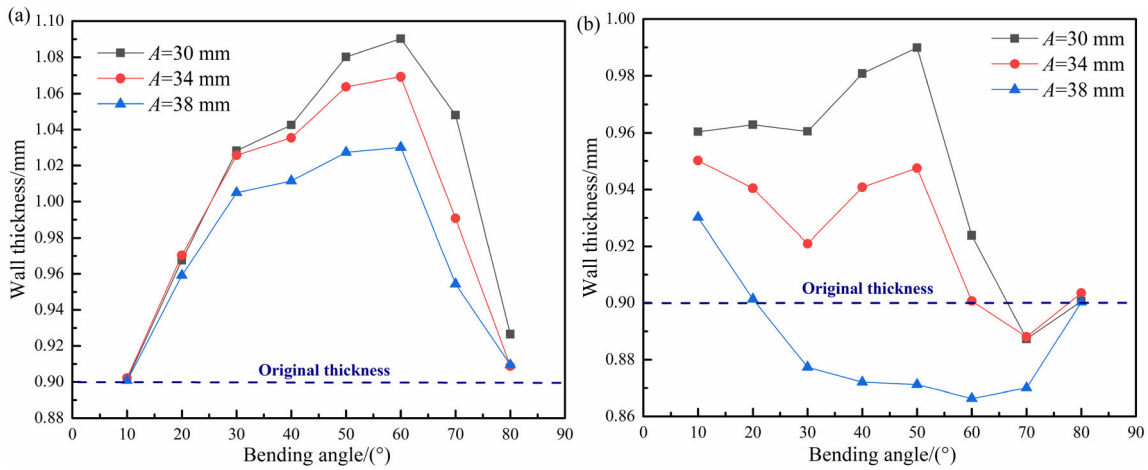

Fig. 17 Evolution of wall thickness of bent tubes with different A. **a** Intrados; **b** extrados

bending die on the bent tube is hardly affected by $\boldsymbol{R_1}$, and A hardly changes with $\boldsymbol{R_1}$. In addition, the equivalent stress in the transition element of bent tube is greater than that in the stable arc element of bent tube. According to the schematic diagram of transition element formation, as shown in Fig. 3, the bent tube in the transition section is subjected to the bending forming force from the bending die, and the dynamic contact between the bent tube and the bending die results in the greater stress concentration on the outer side of bent tube.

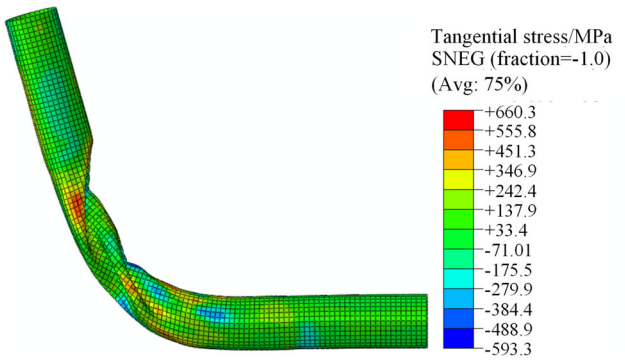

Fig. 18 Simulated bent tube with *A* of 26 mm

The simulated equivalent strain of bent tube with different $\boldsymbol{R_1}$ radii is shown in Fig. 20. During the free bending process, the equivalent strain of bent tube decreases slightly with increasing $\boldsymbol{R_1}$, which means that the degree of plastic deformation of the bent tube decreases slightly and the bending radius of bent tube is almost constant with increasing $\boldsymbol{R_1}$. When other process parameters are the same, the free bending forming limit of the bent tube is hardly affected by $\boldsymbol{R_1}$. However, when $\boldsymbol{R_1}$ is too small, it is easy to cause the stress concentration in the bending arc, resulting in these defects like the deformation accumulation or the indentation on the surface of bent tube near the filleted corner of bending die.

The simulated wall thickness distributions of bent tubes with different $\boldsymbol{R_1}$ radii are displayed in Fig. 21. It was found that the wall thickness distribution on the inside and outside of bent tube hardly changes with $\boldsymbol{R_1}$. In the process of free bending, the bent tube located between the bending die and the guider is subjected to the propulsion from the feeding device and the bending forming force exerted by the bending die. With the increase in $\boldsymbol{R_1}$, the stress state of the bent tube between the bending die and the guider remains constant, and the influence of $\boldsymbol{R_1}$ on the wall thickness might be ignored. The measurement results of wall thickness with different $\boldsymbol{R_1}$ are shown in Fig. 22. It could be concluded that the process of thickening and thinning of the wall thickness of bent tube mainly occurs in the motion stage of the bending die, including the first transition element and the second transition element, as shown in Fig. 3. In the stable arc element of bent tube, there is little variation in the wall thickness distribution. The thickness distribution of the stable arc element on the extrados and intrados of bent tube is hardly affected by $\boldsymbol{R_1}$.

The influence of $\boldsymbol{R_1}$ on the deformation behavior of bent tube is not obvious. In addition, the stress concentration on the inside of bent tube can be reduced by adopting larger bending die filleted corner. Therefore, the smaller $\boldsymbol{R_1}$ should be avoided as much as possible, which can effectively reduce the indentation on the inside of bent tube.

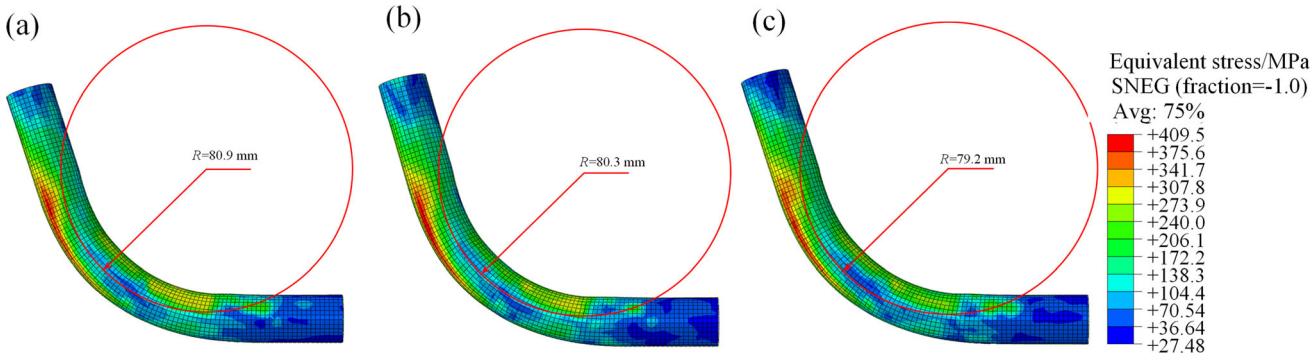

Fig. 19 Equivalent stress distribution cloud maps of bent tubes with different $\boldsymbol{R_1}$ radii. **a** $\boldsymbol{R_1}$ = 1.5 mm; **b** $\boldsymbol{R_1}$ = 3.0 mm; **c** $\boldsymbol{R_1}$ = 4.5 mm

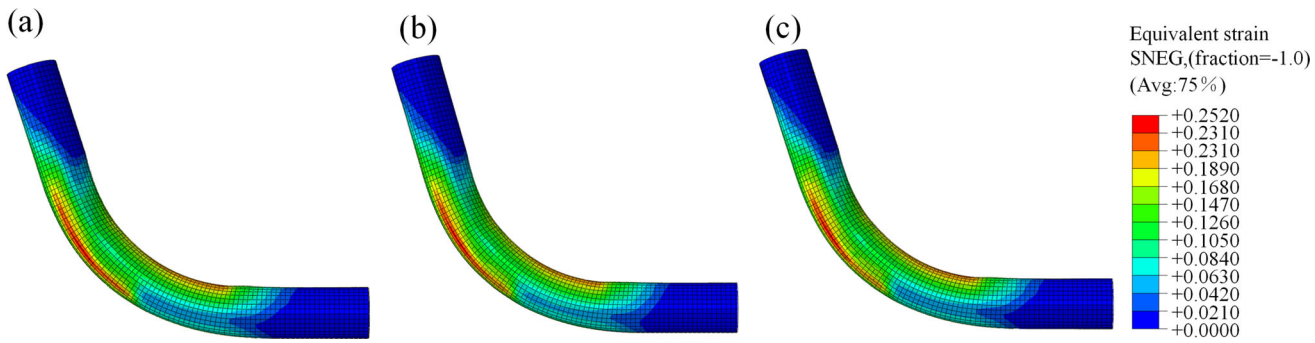

Fig. 20 Equivalent strain distribution cloud maps of bent tubes with different $\boldsymbol{R_1}$ radii. **a** $\boldsymbol{R_1}$ = 1.5 mm; **b** $\boldsymbol{R_1}$ = 3.0 mm; **c** $\boldsymbol{R_1}$ = 4.5 mm

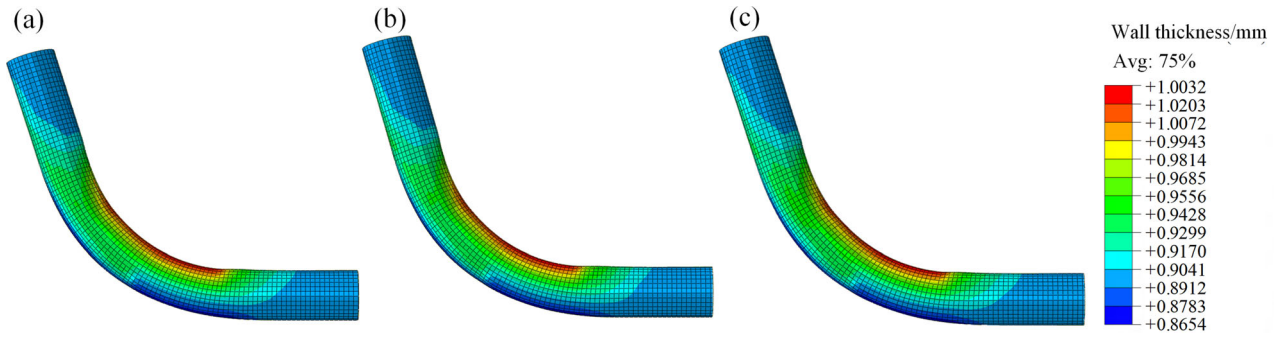

Fig. 21 Wall thickness distribution cloud maps of bent tubes with different R_1 radii. **a** R_1 = 1.5 mm; **b** R_1 = 3.0 mm; **c** R_1 = 4.5 mm

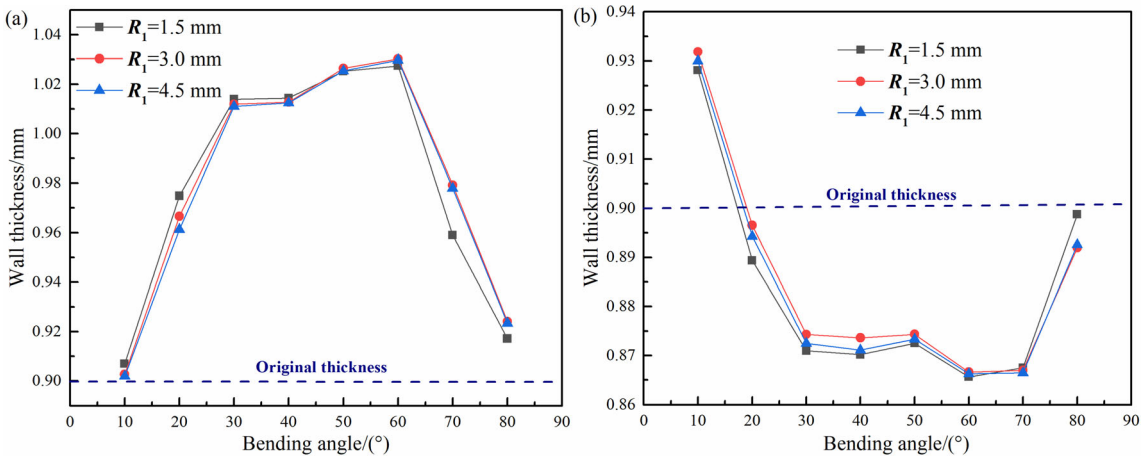

Fig. 22 Evolution of wall thickness of bent tubes with different R_1 radii. **a** Intrados; **b** extrados

4.3 Influence of R_2 on deformation behavior

The simulated equivalent stress and strain of bent tube with different R_2 radii are shown in Figs. 23 and 24. Similar to the evolution law of the equivalent stress and strain on the inside and outside of bent tubes with A, both the maximum stress and strain increase with decreasing R_2. This may be because the distance A increases as R_2 increases, and the restraint effect of guider on bent tube decreases with the increase in R_2. In addition, the bending radius of bent tube increases with increasing R_2 during the free bending process, and the corresponding degree of plastic deformation is weakened. It could be concluded that the free bending forming limit of bent tube is slightly improved by reducing R_2.

The simulated wall thickness of bent tubes with different R_2 radii is shown in Fig. 25. The thickening of thickness on the inner sidewall of bent tubes was promoted, and the thinning of thickness on the outer sidewall of bent tubes was suppressed with the decrease in R_2. This is because the

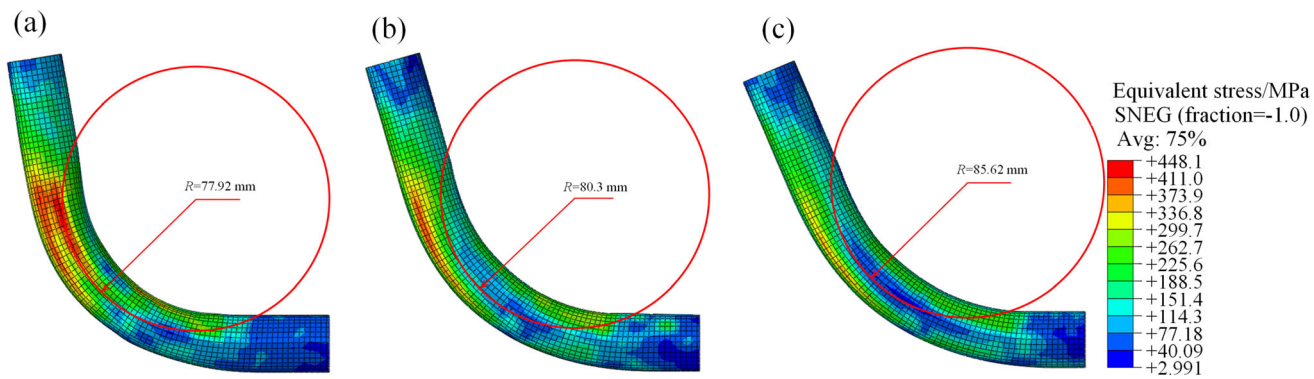

Fig. 23 Equivalent stress distribution cloud maps of bent tubes with different R_2 radii. **a** R_2 = 22 mm; **b** R_2 = 42 mm; **c** R_2 = 62 mm

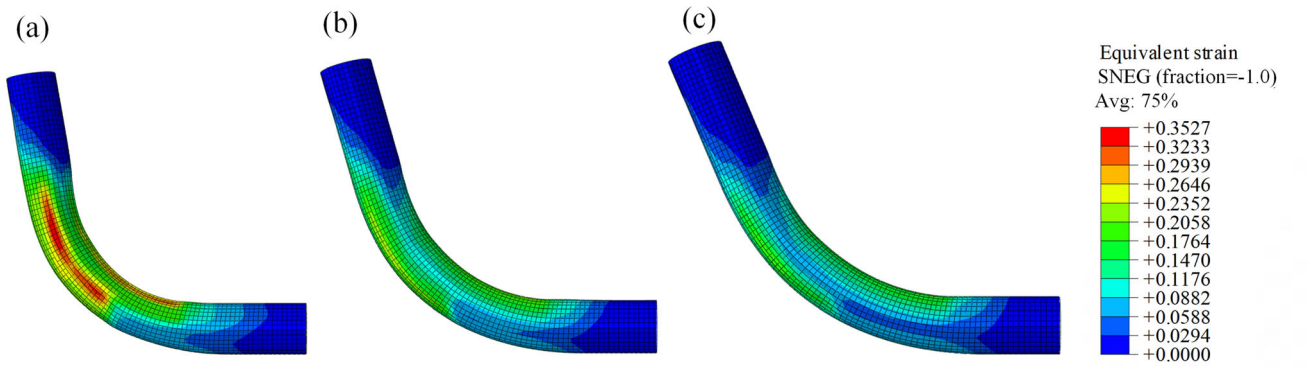

Fig. 24 Equivalent strain distribution cloud maps of bent tubes with different R_2 radii. **a** R_2 = 22 mm; **b** R_2 = 42 mm; **c** R_2 = 62 mm

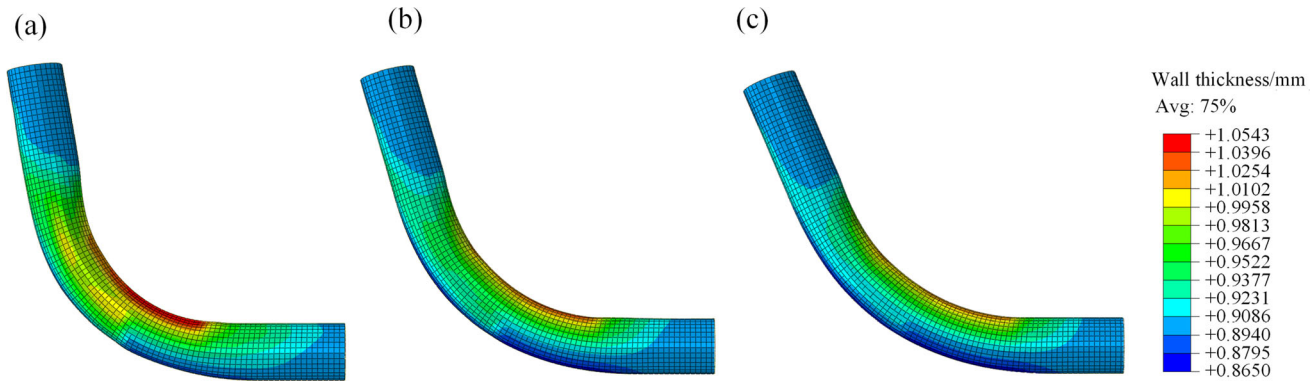

Fig. 25 Wall thickness distribution cloud maps of bent tubes with different R_2 radii. **a** R_2 = 22 mm; **b** R_2 = 42 mm; **c** R_2 = 62 mm

distance A decreases as R_2 decreases, resulting in an increase in the degree of plastic deformation of bent tube. The bent tube is subjected to the axial propulsion from the feeding device, which increases with the decrease in R_2. The tensile stress on the outside of bent tube with smaller R_2 decreases, and the thinning of thickness on the outer sidewall of bent tubes is reduced.

The measurement results of wall thickness on the outside and inside of bent tubes with different R_2 radii are shown in Fig. 26. It could be observed that the thickening of wall thickness on the intrados of bent tube is more obvious as R_2 decreases, which may be attributed to the additional tangential compressive stress on the intrados of bent tube. As shown in Fig. 27b, the tangential

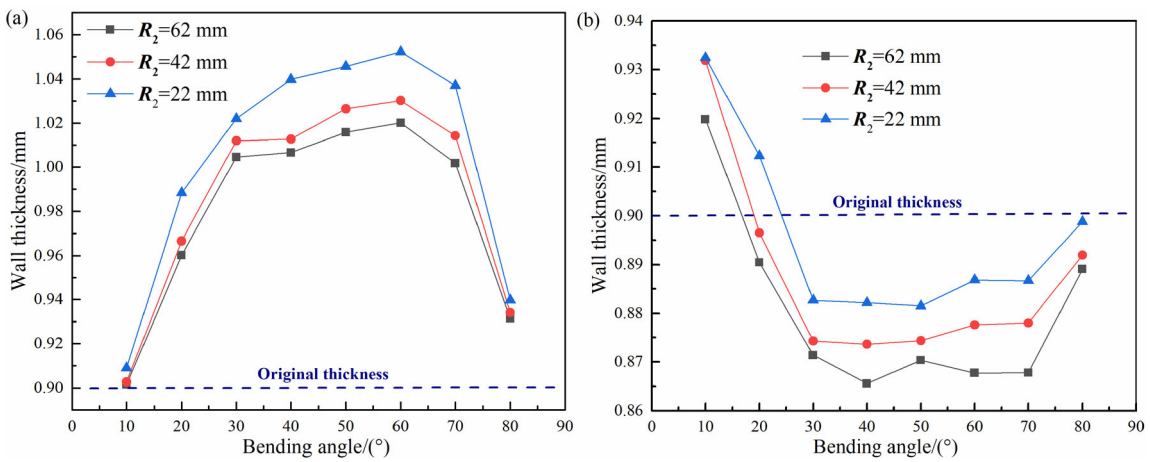

Fig. 26 Evolution of wall thickness of bent tubes with different R_2 radii. **a** Intrados; **b** extrados

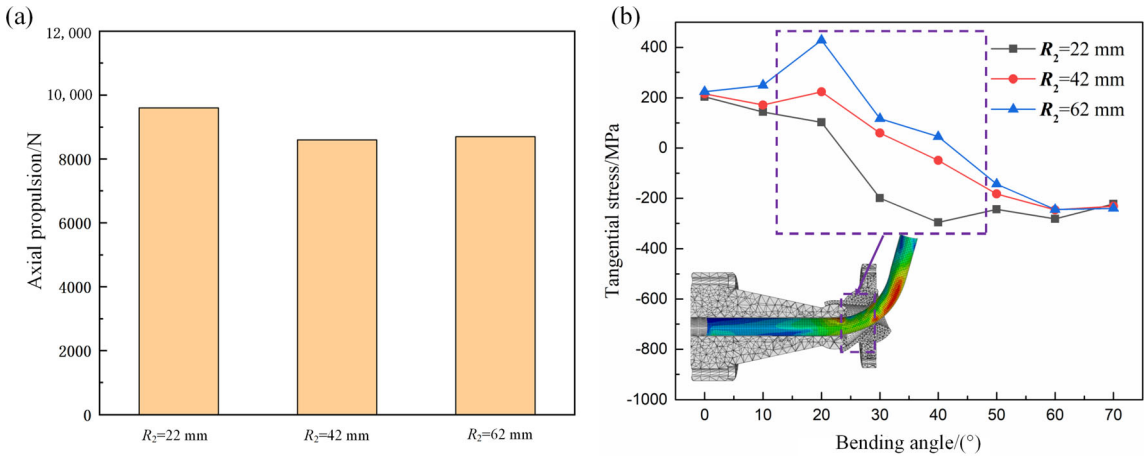

Fig. 27 Axial propulsion (**a**) and tangential stress (**b**) of bent tubes with different R_2 radii

compressive stress increases with decreasing R_2, resulting in more obvious thickening on the intrados of bent tube. The evolution law of axial propulsion exerted by the feeding device on the bent tube with R_2 is shown in Fig. 27a. When R_2 is smaller, the axial propulsion is relatively large, which further leads to the increase in the compressive stress on the intrados of bent tube and the thickening of wall thickness. It was also concluded from Fig. 26 that the maximum thickening rate of the wall thickness of bent tube with R_2 of 22 mm is 16.9%. According to the simulation results, the thinning trend of wall thickness on the outside of bent tubes decreases as R_2 decreases. In general, the plastic deformation of bent tube becomes gentler, and the strain distribution on the inside and outside of bent tube is more uniform with the increase in R_2. However, the corresponding deformation degree of bent tubes decreases, and the bending radius increases. The influence of R_2 on the deformation behavior of bent tube is weaker than that of A. Therefore, the free bending forming limit of bent tube can be improved by appropriately reducing R_2 without the occurrence of these defects, such as wrinkling and cracking.

In general, the effect of R_2 on the free bending forming limit and forming quality of bent tube is similar to that of the distance A. This may be attributed to the fact that the decrease in R_2 would lead to the decrease in A, resulting in more severe local plastic deformation. However, the bending radius of bent tube hardly decreases any more with the further decrease in R_2. Figure 28 shows the simulated defect-free bent tube with R_2 of 18 mm. It was found that the ultimate bending radius of bent tube with R_2 of 18 mm is close to that with R_2 of 22 mm, which is smaller than that with R_2 of 42 mm. As R_2 is further reduced, the stress concentration phenomenon is more obvious during the free bending process and the wear is more likely to occur. Therefore, R_2 is set as 22 mm to reduce the ultimate

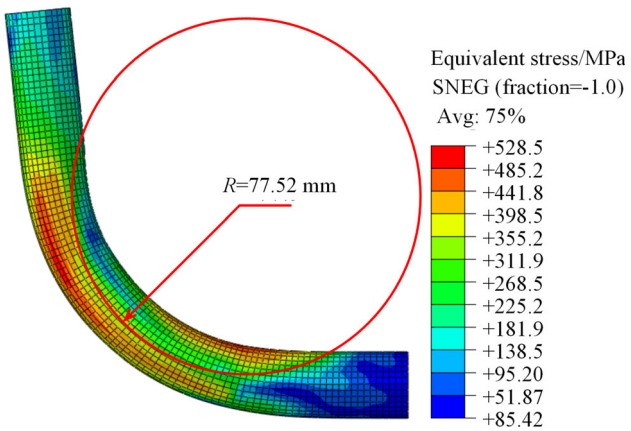

Fig. 28 Simulated defect-free bent tube with R_2 of 18 mm

bending radius of bent tube and improve the forming quality of free bending.

4.4 Verification on newly determined die structure parameters

According to the above analysis results, A and radius of R_2 may be appropriately reduced, while radius of R_1 can be appropriately increased to improve the free bending forming limit and forming quality of bent tube. In this research, the newly determined die structure parameters including A, R_1 radii and R_2 radii were set as 30, 4.5 and 22 mm, respectively. The corresponding free bending dies were designed and manufactured, as shown in Fig. 29. To reduce the scuffing defects on the surface of bent tube and improve the forming quality in the free bending process, the ceramic bushing was adopted in the new free bending dies. The influence of friction on the free bending deformation behavior of bent tube is ignored in this study. The impact of die structure parameters on the free bending forming limit was explored by the experiments. The

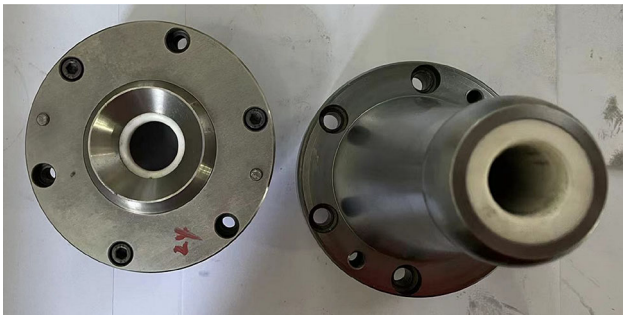

Fig. 29 Free bending dies with newly determined die structure parameters

experimental bent tubes with U of 13 mm are shown in Fig. 30. It was found that the bending radius of bent tube using the newly determined die structure parameters is smaller than that with the original die structure parameters when U is the same. And there is the wrinkling defect on the inside of bent tube with the original die structure parameters. The ultimate bending radius of bent tube for the free bending experiment is reduced, and the free bending forming limit is improved by using the newly determined die structure parameters.

In addition, the experimental cross-sectional distortion rate and the wall thickness of bent tube are concluded in Figs. 31 and 32. Due to the wrinkling on the inside of bent tube, the cross-sectional distortion rate and the wall thickness distribution of the bent tube with the original die structure parameters were not measured and compared. As we can find, the cross-sectional distortion rate is slightly improved by adopting the newly determined die structure parameters, but the maximum cross-sectional distortion rate is still less than 8%. In addition, the thickening of wall thickness on the inner side of bent tube is enhanced, and the thickness of the outer sidewall of bent tube is also slightly increased. The above experimental results also

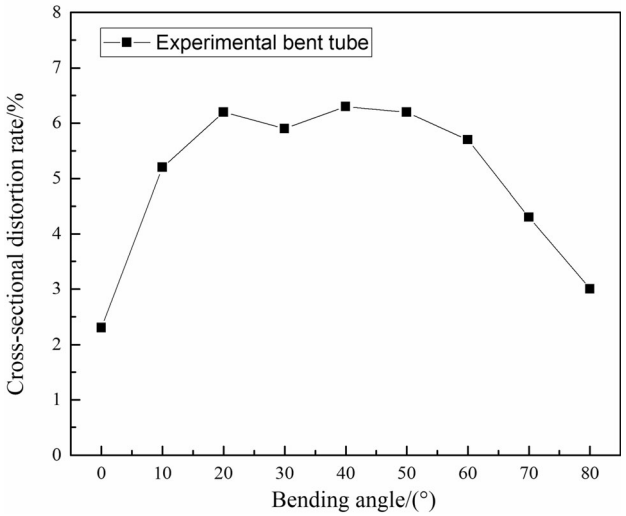

Fig. 31 Cross-sectional distortion rate of experimental bent tube with newly determined die structure parameters

demonstrate the fact that the thinning of wall thickness on the extrados of bent tube is eliminated when A is less than 34 mm. In general, the forming limit of bent tube in the free bending process can be significantly improved, and the corresponding wall thickness variation and the cross-sectional distortion can also be optimized or slightly increased by using the newly determined free die structure parameters.

The free bending deformation behavior of stainless steel tube with the diameter of 22 mm was studied, and the determination principle of die structure parameters was also explored. The free bending forming limit of bent tube can be improved when A is set to 30 mm for the tube with the diameter of 22 mm. The ratio of A to tube diameter is 1.36, which could be used in the process of designing free bending die for these tubes with other diameters. For $\boldsymbol{R_2}$, it might also be determined by the ratio of $\boldsymbol{R_2}$ radii to tube

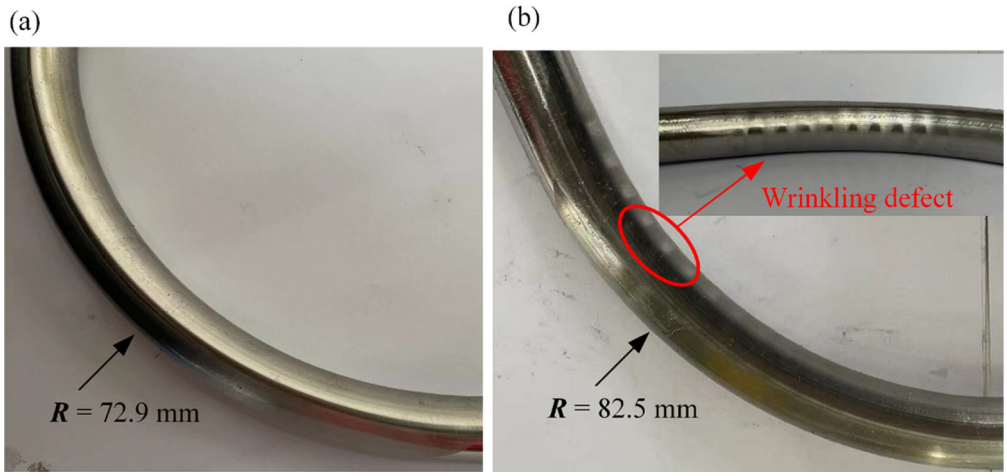

Fig. 30 Experimental bent tubes. **a** Newly determined die structure parameters; **b** original die structure parameters

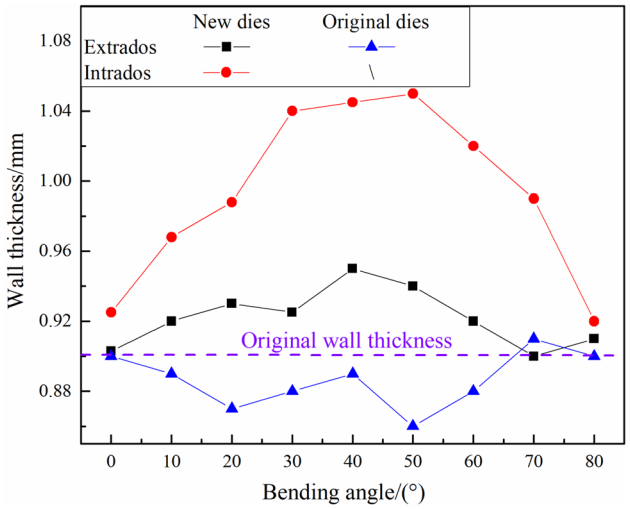

Fig. 32 Wall thickness distribution of experimental and simulated bent tubes with newly determined and original die structure parameters

diameter. Since $\boldsymbol{R_1}$ has little effect on the bending deformation behavior of tube, $\boldsymbol{R_1}$ radii of 4.5 mm may be used as a reference for these tubes with other diameters. For other tubes with the different material properties, the die structure parameters determined above might be employed, but the specific optimization results needs to be further considered and analyzed due to their different springback behaviors.

5 Conclusions

1. The axis of bent tube can be divided into five parts, including the linear segment, the first transition element, the stable arc element, the second transition element and the following linear segment, which correspond to the different movement modes of bending die.
2. The distance between the center point of bending die and the front end of guider along *Z*-axis has an obvious effect on the deformation behavior of bent tubes. The degree of plastic deformation of bent tube is increased, and the uniformity of thickness distribution is improved with the decrease in the distance. The free bending forming limit of bent tube can be improved when the distance is set to 30 mm.
3. The influence of the filleted corner of bending die on the free bending deformation behavior of bent tube is almost insignificant. The stress and strain distribution of bent tube with the different filleted corners of bending die is relatively close, and the evolution of thickness of bent tubes is hardly affected by the filleted corner of bending die. To reduce the stress concentration on the inside of bent tube, the filleted corner of bending die is set to 4.5 mm.
4. The influence of the filleted corner of guider on the deformation behavior of bent tube is between the distance between the center point of bending die and the front end of guider along *Z*-axis and the filleted corner of bending die. The maximum equivalent stress and strain of bent tubes increase with the decrease in the filleted corner of guider, which is set as 22 mm to reduce the ultimate bending radius of bent tube.

Acknowledgements The investigation was supported from the Opening Project of State Key Lab of Digital Manufacturing Equipment & Technology (No. DMETKF2021004), the National Natural Science Foundation of China (Nos. 52105360, U1937206, and 52175328), 2021 Jiangsu Shuangchuang Talent Program (JSSCBS20210157) and Fundamental Research Funds for the Central Universities (No. NS2022061).

Declarations

Conflict of interest The authors declare that they have no known competing financial interests or personal relationships that could have appeared to influence the work reported in this paper.

References

[1] X.S. Bai, Aeronaut. Manuf. Technol. (2014) No. 14, 83–85.
[2] X.Z. Guo, Y. Xu, J. Tao, S.H. Zhang, Advanced cold forming technology for metal hollow components, Science Press, Beijing, China, 2019.
[3] B. Sun, M.X. Qiu, J. Tian, F. Shi, Aeronaut. Manuf. Technol. (2015) No. Z2, 124–128.
[4] Z.X. Zhang, Research on the rotation bending processing of AZ61 magnesium alloy tube, Jilin University, Changchun, China, 2016.
[5] T. Wen, X.W. Ji, Hot Work. Technol. 39 (2010) No. 19, 111–113+117.
[6] D. Shim, K. Kim, K. Lee, J. Mater. Process. Technol. 236 (2016) 189–203.
[7] X.Z. Guo, J. Tao, H. Wang, J. Nanjing Univ. Aeronaut. Astronaut. 52 (2020) 12–23.
[8] M. Murata, T. Kuboki, in: A. Tekkaya, W. Homberg, A. Brosius (Eds.) 60 Excellent inventions in metal forming, Springer Vieweg, Berlin, Heidelberg, 2015, pp. 363–368.
[9] M. Murata, N. Ohashi, H. Suzuki, Trans. Jpn. Soc. Mech. Eng. C 55 (1989) 2488–2492.
[10] M. Murata, J. Jpn. Soc. Technol. Plast. 37 (1996) 515–520.
[11] M. Murata, J. Jpn. Inst. Light Metals 46 (1996) 626–631.
[12] P. Gantner, H. Bauer, D.K. Harrison, A.K.M. De Silva, J. Mater. Process. Technol. 167 (2005) 302–308.
[13] P. Gantner, D.K. Harrison, A.K. De Silva, H. Bauer, Proc. Inst. Mech. Eng. Part B J. Eng. Manuf. 221 (2007) 163–171.
[14] S. Kawasumi, Y. Takeda, D. Matsuura, Trans. JSME 80 (2014) TRANS0343.
[15] S. Chatti, M. Hermes, A.E. Tekkaya, M. Kleiner, CIRP Ann. 59 (2010) 315–318.
[16] H. Xiong, Resesrch on the forming limit of free bending process of metal tubes, Nanjing University of Aeronautics and Astronautics, Nanjing, China, 2019.

[17] P. Li, L. Wang, M. Li, Int. J. Adv. Manuf. Technol. 88 (2017) 1669–1675.
[18] P. Li, L. Wang, M. Li, Int. J. Adv. Manuf. Technol. 87 (2016) 2853–2859.
[19] Z.K. Zhang, J.J Wu, B. Liang, M.Z. Wang, J.Z. Yang, M. Muzamil, J. Mater. Process. Technol. 282 (2020) 116662.
[20] X.Z. Guo, C. Cheng, J.X. Guo, H. Zhang, H. Chen, C.M. Liu, Forging & Stamping Technology 46 (2021) No. 4, 127–136.
[21] X. Chen, X.Z. Guo, J. Tao, Y. Xu, A. Abd El-Aty,, H. Liu, Int. J. Mech. Sci. 160 (2019) 103–113.
[22] H. Chen, H. Wang, A. Abd El-Aty, Y. Qin, J. Li, Y. Zhang, T. Li, X. Guo, Chin. J. Aeronaut. 34 (2021) No. 4, 253–264.
[23] Q.L. Meng, Study on swing mould of joint swing type free pipe bending process, Yanshan University, Qinhuangdao, China, 2019.
[24] X.Z. Guo, H. Xiong, H. Li, Y. Xu, Z.Q. Ma, A. Abd El-Aty, Y.N. Ma, K. Jin, Int. J. Mach. Tools Manuf. 133 (2018) 72–84.
[25] J.J. Wu, Z.K. Zhang, Chin. J. Aeronaut. 34 (2021) No. 11, 267–276.
[26] D. Maier, S. Stebner, A. Ismail, M. Dölz, B. Lohmann, S. Münstermann, W Volk. Adv. Ind. Manuf. Eng. 2 (2021) 100047.
[27] R. Hashemi, S.A. Niknam, J. Manuf. Process. 56 (2020) 390–399.
[28] X. Guo, W. Wei, Y. Xu, A. Abd El-Aty, H. Liu, H. Wang, X. Luo, J. Tao, Int. J. Mech. Sci. 150 (2019) 12–19.